Effect of Modulating FcRn Binding on Direct and Pretargeted Tumor Uptake of Full-length Antibodies

Lidia Nazarova[1], Hanine Rafidi[1], Danielle Mandikian[1], Gregory Z. Ferl[1,2], James T. Koerber[3], Christopher W. Davies[3], Sheila Ulufatu[4], Jason Ho[4], Jeffrey Lau[5], Shang-Fan Yu[5], James Ernst[6], Jack D. Sadowsky[6], and C. Andrew Boswell[1]

ABSTRACT

Full-length antibodies lack ideal pharmacokinetic properties for rapid targeted imaging, prompting the pursuit of smaller peptides and fragments. Nevertheless, studying the disposition properties of antibody-based imaging agents can provide critical insight into the pharmacology of their therapeutic counterparts, particularly for those coupled with potent payloads. Here, we evaluate modulation of binding to the neonatal Fc receptor (FcRn) as a protein engineering-based pharmacologic strategy to minimize the overall blood pool background with directly labeled antibodies and undesirable systemic click reaction of radiolabeled tetrazine with circulating pretargeted *trans*-cyclooctene (TCO)-modified antibodies. Noninvasive SPECT imaging of mice bearing HER2-expressing xenografts was performed both directly (^{111}In-labeled antibody) and indirectly (pretargeted TCO-modified antibody followed by ^{111}In-labeled tetrazine). Pharmacokinetic modulation of antibodies was achieved by two distinct methods: Fc engineering to reduce binding affinity to FcRn, and delayed administration of an antibody that competes with binding to FcRn. Tumor imaging with directly labeled antibodies was feasible in the absence of FcRn binding, rapidly attaining high tumor-to-blood ratios, but accompanied by moderate liver and spleen uptake. Pretargeted imaging of tumors with non-FcRn-binding antibody was also feasible, but systemic click reaction still occurred, albeit at lower levels than with parental antibody. Our findings demonstrate that FcRn binding impairment of full-length IgG antibodies moderately lowers tumor accumulation of radioactivity, and shifts background activity from blood pool to liver and spleen. Furthermore, reduction of FcRn binding did not eliminate systemic click reaction, but yielded greater improvements in tumor-to-blood ratio when imaging with directly labeled antibodies than with pretargeting.

Introduction

The prolonged serum persistence of target-specific antibodies has provided numerous therapeutic agents with favorable pharmacologic properties, so that weekly to near monthly dosing is common (1, 2). However, the slow systemic clearance of antibodies is a double-edged sword since wait times of days are needed until target-to-blood ratios become optimal (3, 4). For diagnostic imaging, this limitation has been addressed by pursuing smaller, faster clearing antibody fragments such as Fabs (5–7), minibodies (8), or diabodies (9), all lacking the Fc region of the antibody responsible for neonatal Fc receptor (FcRn)-mediated recycling. These same-day imaging agents have overcome the slow pharmacokinetics of immunoPET/SPECT imaging agents comprised of full-length antibodies, thus benefiting patient convenience, compliance, diagnosis time, and radiation dosimetry.

Although this "smaller/faster" strategy decreases serum persistence, it also shifts radioactivity away from target receptors and towards clearance organs, particularly kidneys, which can result in dose-limiting radiotoxicity (10). Using nonresidualizing radiolabels (e.g., ^{124}I, ^{18}F) and/or metabolically labile linkers can overcome high renal dosimetry (11), but at the expense of losing the residualization advantage within tumor/target tissues for internalizing receptors. Furthermore, these liabilities raise similar concerns in the pharmacologic context of the corresponding biotherapeutic agents, particularly those coupled with potent payloads, so that both systemic exposure and normal tissue uptake/catabolism are intimately linked to therapeutic index.

Recently, pretargeted imaging via *in vivo* click chemistry has been investigated as an alternative approach to address the undesirably slow pharmacokinetics of antibody-based imaging agents (12, 13). The implications of this technology on therapeutic drug delivery have also been explored (14), but several limitations remain. Tumor-to-background ratios in pretargeted imaging are typically better for slow/noninternalizing targets than for internalizing targets. For instance, we previously demonstrated that same-day imaging of pretargeted anti-HER2 (internalizing) antibodies was inferior to imaging with directly labeled antibodies, as substantial levels of systemic click reaction limited delineation of tumors from blood pool background (15). Furthermore, antibody pretargeting often benefits from clearing/blocking agents to reduce systemic reaction/labeling (16), but this adds another step that could be disadvantageous from an operational viewpoint.

Here, we further pursue a protein engineering strategy to modulate antibody pharmacokinetics by lowering FcRn binding affinity to achieve rapid target delineation. Previously, ^{124}I-labeled scFv-Fc variants (~105 kDa) were employed in slow-internalizing receptor

[1]Preclinical and Translational Pharmacokinetics, Genentech Research and Early Development, South San Francisco, California. [2]Biomedical Imaging, Genentech Research and Early Development, South San Francisco, California. [3]Antibody Engineering, Genentech Research and Early Development, South San Francisco, California. [4]In Vivo Studies, Genentech Research and Early Development, South San Francisco, California. [5]Translational Oncology, Genentech Research and Early Development, South San Francisco, California. [6]Protein Chemistry, Genentech Research and Early Development, South San Francisco, California.

Note: Supplementary data for this article are available at Molecular Cancer Therapeutics Online (http://mct.aacrjournals.org/).

L. Nazarova and H. Rafidi contributed equally to this article.

Corresponding Author: C. Andrew Boswell, Genentech Inc., 1 DNA Way, MS 463A, South San Francisco, CA 94080. Phone: 650-467-4603; Fax: 650-742-5234; E-mail: boswell.andy@gene.com

Mol Cancer Ther 2020;19:1052–8

doi: 10.1158/1535-7163.MCT-19-1015

models in an imaging context (17–19). We have instead chosen to evaluate a full-length IgG (~150 kDa) with a residualizing label (^{111}In) in an internalizing target (HER2) expressing tumor model using immunoSPECT as a readout but with intended therapeutic implications.

To directly assess the impact of FcRn-mediated IgG recycling and the resulting impact on serum persistence and tumor-to-background ratio, we evaluated the presence and absence of FcRn binding activity using two methods: Fc engineering of intact IgG to ablate FcRn binding (20) and administration of a competitive FcRn binding antibody, effectively acting as a clearing agent, with engineered Fc mutations (YTE-KF) to enhance FcRn binding as described in a previous report of the "ABDEG" antibody (21, 22). We investigated these two approaches in the context of both direct and pretargeted imaging, taking advantage of the click reaction between *trans*-cyclooctane (TCO)-modified antibodies and radiolabeled tetrazines.

Materials and Methods

All animal studies were conducted in accordance with the guidelines of the American Association for Accreditation of Laboratory Animal Care and the Genentech Institutional Animal Care and Use Committee (IACUC). Details regarding all reagents and general procedures may be found in the Supplementary Information (available at http://mct.aacrjournals.org/).

Antibody engineering and conjugation

Anti-HER2 THIOMAB antibodies (clone 7C2, which binds a different epitope than trastuzumab or pertuzumab; see Supplementary Table S1 for 7C2 sequence as previously reported in ref. 23) were engineered to introduce cysteine residues at three positions (24) for conjugation to the click-reactive TCO-PEG$_3$-maleimide (polyethylene glycol, PEG) linker (25, 26), the metal chelator DOTA-maleimide (1,4,7,10-tetraazacyclododecane-1,4,7-tetraacetic acid, DOTA) for imaging via ^{111}In-DOTA$_6$-mAbs, and the capping reagent *N*-ethyl maleimide (NEM) as described previously (15) to give final conjugates with ~6 TCO, DOTA, or NEM groups per antibody (Supplementary Table S2). These cysteine mutations were engineered alone or in combination with additional mutations—H310A/H435Q—to ablate binding to FcRn (20). Selected groups of mice received an anti-gD YTE-KF hIgG1 antibody, a competitive binder to FcRn, with the same mutations as the "ABDEG" antibody reported previously (21, 22) and featuring single-digit nanomolar affinity to mouse FcRn at both pH 6.0 and 7.2 (21).

Radiochemistry and chromatography

7C2-NEM$_6$, 7C2-HAHQ-NEM$_6$, 7C2-TCO$_6$, and 7C2-HAHQ-TCO$_6$ antibodies were radioiodinated (^{125}I) for invasive biodistribution assessment through tyrosine residues (Supplement S1; refs. 15, 27). Radiosynthesis of ^{111}In-DOTA$_6$-labeled 7C2 and 7C2-HAHQ for direct imaging was achieved via engineered thiols (Supplement S2; ref. 15); in addition, ^{111}In-DOTA-Tz was synthesized (Supplement S3) for pretargeted imaging (15, 28).

SPECT-CT imaging

The KPL-4 tumor-bearing C.B-17 SCID.bg mouse model (mean tumor volume at least 250 mm^3) was utilized as described previously (15). An overview of the SPECT-CT imaging study design is presented in **Fig. 1**. All dosing was single intravenous (tail vein) bolus in sterile saline vehicle (100 µL), with all antibody tracers adjusted with unlabeled protein to 5 mg/kg total dose. Directly labeled groups received 185 kBq of ^{125}I-7C2-NEM$_6$ plus 11.1 MBq ^{111}In-DOTA$_6$-7C2 (group 1) or 185 kBq of ^{125}I-7C2-HAHQ-NEM$_6$ plus 11.1 MBq ^{111}In-DOTA$_6$-7C2-HAHQ (group 2), each followed 24 hours later by vehicle. *In vivo* click reactions were performed by administering 185 kBq of ^{125}I-7C2-TCO$_6$ (group 4) or ^{125}I-7C2-HAHQ-TCO$_6$ (group 5) followed 24 hours later by 11.1 MBq ^{111}In-DOTA-Tz. Selected groups received ^{111}In-DOTA$_6$-7C2 (group 3) or ^{125}I-7C2-TCO$_6$ (group 6) followed 24 hours later by IgG-YTE-KF (50 mg/kg), thereafter by vehicle or ^{111}In-DOTA-Tz at 48 hours after initial injection.

SPECT images were acquired in two 20% windows centered at the 173- and 247-keV photopeaks of ^{111}In using an ultra-high sensitivity mouse 2.0-mm-pinhole collimator (MILabs). For each animal, two frames (15 minutes each) were acquired. Image reconstruction and coregistration (MILabs software), SPECT quantitation (VivaQuant software), and visualization (Amira software) were performed.

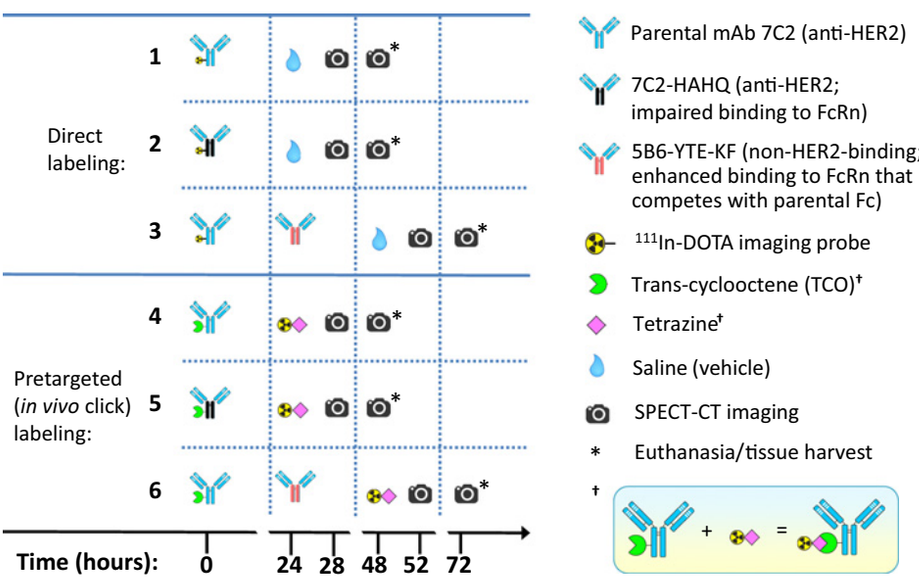

Figure 1.
Schematic overview of imaging study design. The numbering of groups 1 to 6 is maintained throughout all subsequent figures for clarity and cross-referencing.

Regions of interest were drawn around heart (surrogate for blood exposure) and tumor, based on CT anatomical images.

Pharmacokinetics and biodistribution

Blood samples from all mice in the SPECT imaging study were collected at 0.25, 24.25, and 48 hours (0.25, 48.25, and 72 hours for the IgG-YTE-KF groups) after initial antibody injection via retroorbital bleed, with terminal tissue harvest performed at 2 days (3 days for the IgG-YTE-KF groups) after initial antibody injection. Tissue samples collected from the terminal harvests included tumor, kidney, liver, spleen, muscle, fat pad, small intestine, skin, heart, lungs, and brain. Tissues collection, analysis, and calculations were performed as described previously (15). Sparse blood pharmacokinetic data were fit to a standard linear two-compartment pharmacokinetic model (Supplement S4; ref. 29).

Results

Antibody engineering and conjugation

DOTA-maleimide, TCO-PEG_3-maleimide, and NEM were conjugated through the engineered thiols of 7C2 (LC: K149C, HC: L177C, HC: Y376C), with >95% efficiency by mass spectrometry. Conjugation ratios are reported in Supplementary Table S2.

Radiochemistry and chromatography

Radioiodination of the antibodies with 37 MBq input gave ~50% yields for ^{125}I-7C2-TCO_6 (~340.4 kBq/μg, 99% pure) and ^{125}I-7C2-HAHQ-TCO_6 (~314.5 kBq/μg, 99% pure), 64% for ^{125}I-7C2-NEM_6 (~510.6 kBq/μg, 98% pure), and 74% for ^{125}I-7C2-HAHQ-NEM_6 (~418.1 kBq/μg, 97% pure). Radiometal labeling of 7C2-$DOTA_6$ and 7C2-HAHQ-$DOTA_6$ antibodies gave 77% yield for ^{111}In-$DOTA_6$-7C2 (~210.9 kBq/μg, 99% pure) and 38% for ^{111}In-$DOTA_6$-7C2-HAHQ (~173.9 kBq/μg, 96% pure), that of DOTA-Tz provided ~71% yield of ^{111}In-DOTA-Tz (8.11 MBq/μg based on amount of tetrazine prior to Sep-Pak, 95% pure; Supplementary Fig. S1).

SPECT-CT imaging

All data in this manuscript were collected in a single comprehensive imaging study (**Fig. 2**), with blood concentrations (**Fig. 3**) derived by sparse sampling, and tissue harvest (**Figs. 4–6**) performed after the last image acquisition. Tumor-to-heart/blood ratios obtained by SPECT/harvest for all groups are available in Supplementary Table S3.

In the direct imaging study arm, good tumor delineation was observed at 28 hours for both parental (7C2) and FcRn nonbinding (7C2-HAHQ) tracers (**Fig. 2**; groups 1–2). The background signal in animals injected with ^{111}In-7C2 was primarily in heart/blood pool, that with ^{111}In-7C2-HAHQ in liver and spleen. Tumor-to-blood ratios were nearly two-fold higher for the HAHQ variant relative to the parental molecule, and two-fold higher at 48 hours (than 24 hours) after antibody injection.

In the pretargeted study arm, the majority of signal was observed in circulation at 4 hours after ^{111}In-DOTA-Tz administration, consistent with tumor-to-blood ratios <1, although with distinguishable tumor

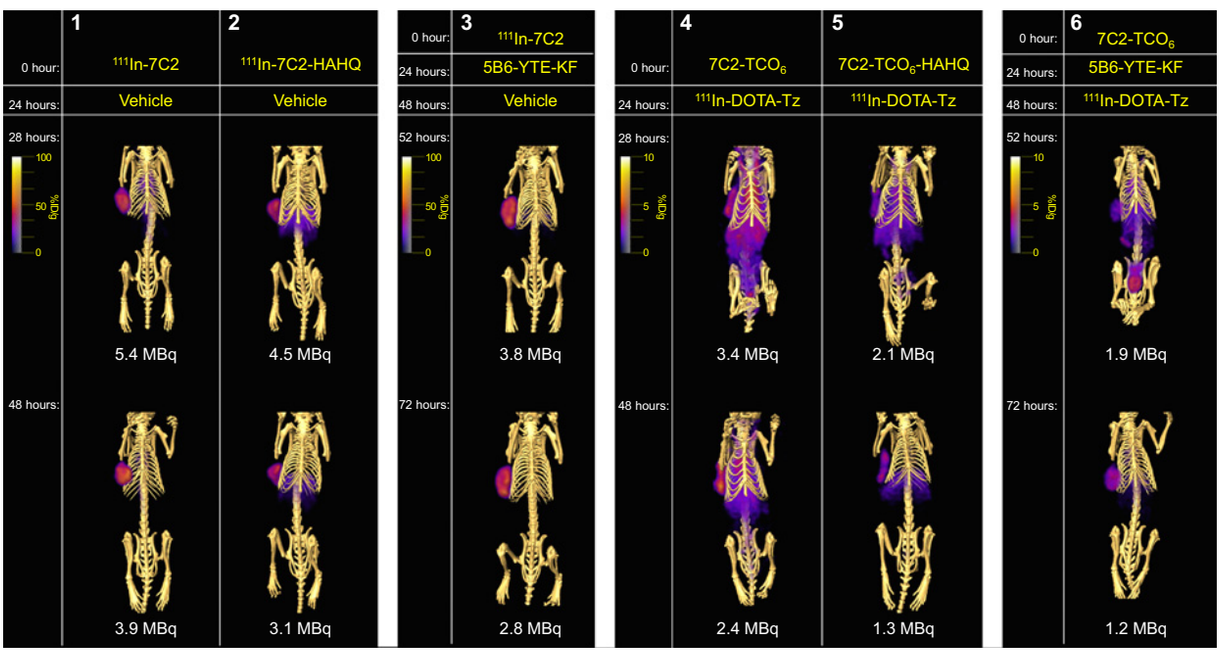

Figure 2.

Representative SPECT-CT images across both direct (^{111}In-DOTA-mAb) and pretargeted (mAb-TCO_6 followed by ^{111}In-DOTA-tetrazine) arms. The color scales apply only to the SPECT image, not the CT skeleton, which is presented in beige for anatomic reference. Note the differences in timing between panels. KPL-4 tumor bearing mice were injected with either directly labeled ^{111}In-DOTA-labeled mAb coinjected with 5 mg/kg unlabeled mAb (direct labeling groups 1–3) or 5 mg/kg of 7C2-TCO_6 antibodies, followed 24 hours (or 48 hours) later by ^{111}In-DOTA-Tz (pretargeting groups 4–6). Imaging was performed at 28 and 48 hours post-^{111}In-DOTA-mAb or mAb-TCO (4 hours post ^{111}In-DOTA-Tz for pretargeted groups) for all groups except those whose time points are shifted 1 day later to accommodate injection by 5B6-YTE-KF (groups 4–6). (All): Total body radioactivity at time of imaging is indicated for each image. Animals from each group were imaged for the same amount of time and images rendered with the same voxel range to indicate relative differences within each group. Vehicle, phosphate-buffered saline; TCO, *trans*-cyclooctene; Tz, tetrazine.

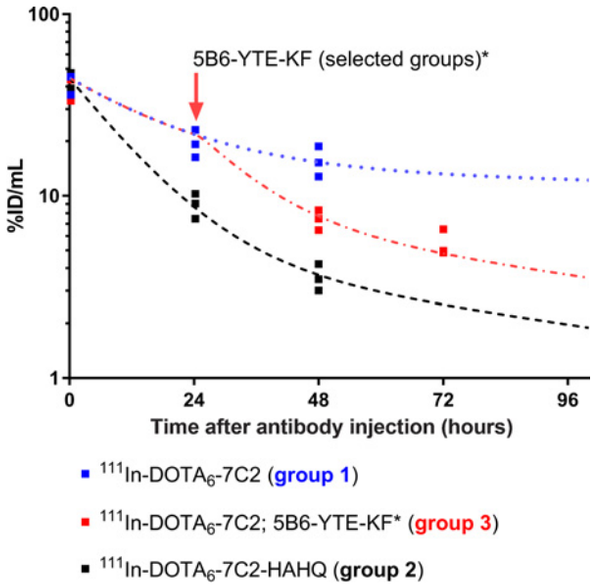

Figure 3.

Sparse pharmacokinetics of ^{111}In-labeled antibodies in the direct labeling arm of the imaging study. Dashed lines are model fits, and symbols are observed data ($n = 3$). (Parental and HAHQ/groups 1–2): KPL-4 tumor bearing mice received 11.1 MBq of ^{111}In-DOTA$_6$-mAb (blue/black). Whole blood was collected at 0.25, 24.25 (15-minute delay to match tetrazine injection timing in groups 4–6) and 48 hours after antibody injection. (YTE-KF/group 3): KPL-4 tumor bearing mice received 11.1 MBq of ^{111}In-DOTA$_6$-mAb (red) followed 24 hours later by 50 mg/kg dose of anti-gD-YTE-KF. Whole blood was collected at 0.25, 48.25, and 72 hours after antibody injection. For model fit, data at 24 hours were assumed to be same as for parental group. (All): Samples were subjected to gamma counting and values were plotted as %ID/mL of blood. ID, injected dose.

delineation (**Fig. 2**; groups 4–5). However, a next-day SPECT scan revealed ∼two-fold increase in tumor-to-blood ratio for both variants relative to same-day imaging.

Mice receiving directly labeled ^{111}In-7C2 followed by anti-gD-YTE-KF demonstrated good tumor delineation at 52 hours, with nearly two-fold increase in tumor-to-blood ratio as compared with ^{111}In-DOTA-7C2-HAHQ (**Fig. 2**; group 3). However, significant blood pool signal was observed for the pretargeted group with anti-gD-YTE-KF, resulting in a similar tumor-to-blood ratio at 52 hours to that of 7C2-HAHQ-TCO$_6$ + ^{111}In-DOTA-Tz group (**Fig. 2**; group 6). The 72-hour SPECT images for direct labeling followed by anti-gD-YTE-KF showed a slight improvement of already well-resolved image (**Fig. 2**; group 3). The pretargeted group followed by anti-gD-YTE-KF also demonstrated better tumor delineation (**Fig. 2**; group 6).

Pharmacokinetics and biodistribution

In the direct labeling study arm, the FcRn-binding impaired variant ^{111}In-DOTA$_6$-7C2-HAHQ exhibited faster systemic clearance than parental ^{111}In-DOTA$_6$-7C2 with the blood concentration being two-fold lower for the HAHQ variant at 24 hours after antibody injection (8.9 ± 1.4 and 19.5 ± 3.4 %ID/mL, respectively; black vs. blue, **Fig. 3**). By 48 hours after antibody injection, the difference in pharmacokinetics between the HAHQ variant and parental antibody was even more dramatic with more than four-fold difference in whole blood of 3.6 ± 0.6 and 15.2 ± 3.0 %ID/mL, respectively (see Supplementary Table S4, for fitted pharmacokinetic parameter values).

A similar discrepancy between HAHQ variants and parental molecules was observed for the co-administered ^{125}I-labeled mAb–NEM$_6$ conjugates in the direct labeling study arm and for the mAb–TCO$_6$ conjugates in the pretargeted arm (black vs. blue, Supplementary Fig. S3). In addition, the clearance of all parental 7C2 antibodies (independent of labeling method or conjugation) increased from the time at which 50 mg/kg anti-gD-YTE-KF was administered due to effective blocking of FcRn by the clearing agent (red, **Fig. 3**; Supplementary Fig. S3).

Pretargeted groups demonstrated rapid blood clearance of ^{111}In label due to the pharmacokinetic properties of the small molecule tracer, ^{111}In-DOTA-Tz (Supplementary Fig. S4). Only 15 minutes after the ^{111}In-DOTA-Tz administration, pretargeted groups showed ∼40% less blood-circulating ^{111}In tracer (on a dose-normalized basis) as compared with the intact antibody (13.6 ± 1.4 vs. 21.8 ± 1.3%ID/mL, respectively; Supplementary Figs. S3 vs. S4). Although there was no dramatic difference in blood levels of ^{111}In-DOTA-Tz between the parental 7C2-TCO$_6$ (blue, Supplementary Fig. S4A) and 7C2-HAHQ-TCO$_6$ (black, Supplementary Fig. S4B) at 15 minutes after tetrazine, the blood level at 24 hours was three times higher in mice receiving parental 7C2-TCO$_6$ than for 7C2-HAHQ-TCO$_6$.

Biodistribution data for ^{111}In-DOTA$_6$-7C2 showed high tumor uptake of the ^{111}In label whether alone (blue, **Fig. 4A**; 48.5%ID/g at 48 hours) or followed by 50 mg/kg anti-gD-YTE-KF (72 hours

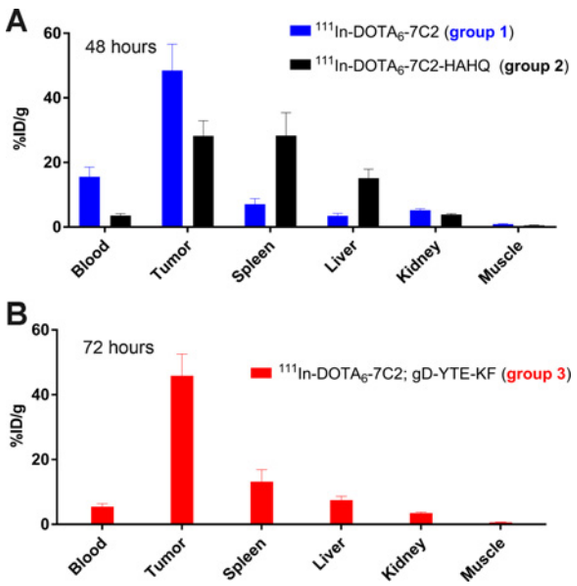

Figure 4.

Tissue distribution (intact plus residualized) for directly (^{111}In-DOTA)-labeled antibodies assessed by tissue harvest after the SPECT imaging study. **A** (parental and HAHQ/groups 1–2): Data included for parental 7C2 antibody (*blue*), the FcRn binding impaired 7C2-HAHQ (*black*) for tissue harvest at 48 hours. **B** (YTE-KF/group 3), Data included for parental 7C2 followed 24 hours later by 50 mg/kg anti-gD-YTE-KF (red) and tissue harvest at 72 hours. (All): KPL-4 tumor-bearing mice were injected with ^{111}In-mAb (11.1 MBq) mixed with 5 mg/kg total mAb. Tissues were harvested, rinsed with saline, weighed, and gamma counted to produce data plotted as %ID/g of tissue. ID, injected dose.

uptake; red, **Fig. 4B**; 45.9%ID/g at 72 hours). In contrast, ^{111}In-DOTA$_6$-7C2-HAHQ showed signal accumulation not only in the tumor (28.2%ID/g) but also significant amounts in the liver (15.1%ID/g) and spleen (28.3%ID/g; black, **Fig. 4A**; 48 hours). Mice receiving ^{111}In-DOTA$_6$-7C2 followed by anti-gD-YTE-KF had 72-hour hepatic and splenic uptake intermediate between the 48-hour levels observed in ^{111}In-DOTA$_6$-7C2 and ^{111}In-DOTA$_6$-7C2-HAHQ groups (**Fig. 4**). Tumor-to-blood ratios by gamma counting largely mirrored those obtained by SPECT during the last image acquisition (Supplementary Table S3).

Similar to the directly labeled groups (**Fig. 4**), 7C2-TCO$_6$ followed by the tetrazine tracer (blue, **Fig. 5A**) demonstrated higher ^{111}In accumulation in the tumor than 7C2-HAHQ-TCO$_6$ (black, **Fig. 5A**; 10.4 ± 1.0 and 6.3 ± 1.0 %ID/g, respectively at 48 hours, ∼1.5-fold) with nearly two-fold higher tumor-to-blood ratio for the latter (Supplementary Table S3); but only modest accumulation in liver and spleen. Results for click reaction of ^{111}In-DOTA-Tz after anti-gD-YTE-KF administration at 72 hours (red, **Fig. 5B**) were similar to the corresponding 7C2-HAHQ-TCO$_6$ group at 48 hours, but with lower tumor, liver, and spleen uptake.

Biodistribution data for ^{125}I-7C2-NEM$_6$ and ^{125}I-7C2-HAHQ-NEM$_6$ (solid blue and black, respectively; Supplementary Fig. S5A) at 48 hours after administration revealed that FcRn binding impairment by point mutations yielded nearly three-fold signal reduction in tumor and most tissues, largely mirroring exposure. Consistent with previous work, far less tumor uptake was observed with the nonresidualizing ^{125}I label than with ^{111}In-DOTA (30). Distribution of ^{125}I-7C2-TCO$_6$ and ^{125}I-7C2-HAHQ-TCO$_6$ (hatched blue and black, respectively; Supplementary Fig. S5A) were similar to that of the ^{125}I-labeled mAb-NEM$_6$ variants in the direct study arm (solid bars). Data for ^{125}I-7C2-NEM$_6$ followed 24 hours later by 50 mg/kg anti-gD-YTE-KF and harvested at 72 hours after administration (red, Supplementary Fig. S5B) was similar to that of ^{125}I-7C2-HAHQ-NEM$_6$ at 48 hours.

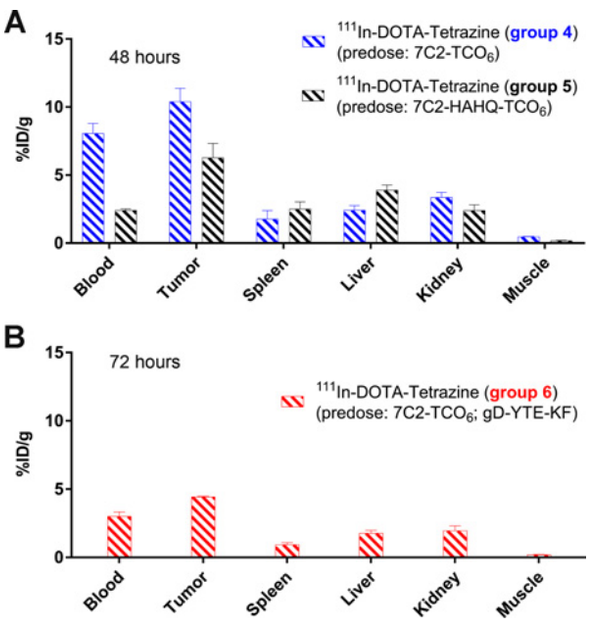

Figure 5.
Tissue distribution data for antibody–TCO conjugates followed by ^{111}In-labeled tetrazine. **A** (parental and HAHQ/groups 4-5), KPL-4 tumor-bearing mice were injected with 5 mg/kg total of mAb-TCO$_6$ followed by ^{111}In-Tz (11.1 MBq) at 24 hours and subsequent tissue harvest at 48 hours. Data are included for the TCO conjugates of parental 7C2 antibody (blue), the FcRn binding impaired 7C2-HAHQ (*black*). **B** (YTE-KF/group 6), KPL-4 tumor-bearing mice were injected with 5 mg/kg total of parental 7C2-TCO$_6$ followed 24 hours later by 50 mg/kg anti-gD-YTE-KF, ^{111}In-Tz (11.1 MBq) at 48 hours (red). Tissue harvest was at 72 hours. (All): Tissues were harvested, rinsed with saline, weighed, and gamma counted to produce data plotted as %ID/g of tissue. Data are tracking ^{111}In-DOTA-Tz (residualizing), a portion of which has click reacted with mAb-TCO$_6$. ID, injected dose; TCO, *trans*-cyclooctene.

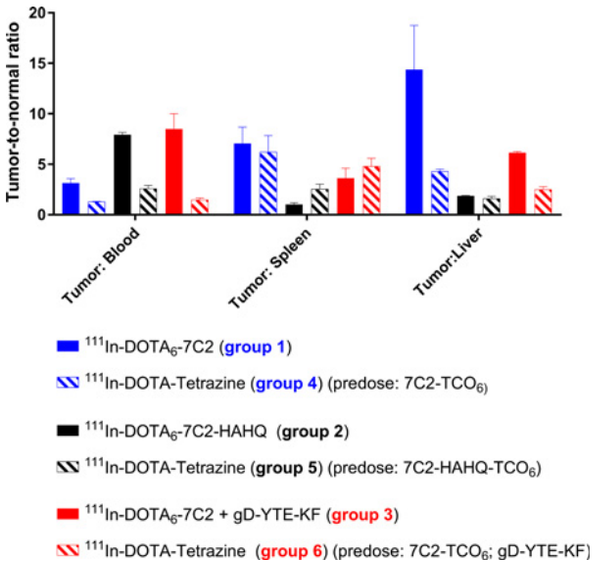

Figure 6.
Tumor-to-background ratios of %ID/g values achieved at last imaging time point (48 hours; 72 hours for groups receiving YTE-KF) across all treatment groups. TCO, *trans*-cyclooctene.

Discussion

Our primary goal was to compare two methods, direct FcRn binding attenuation via site mutagenesis and use of a competitive FcRn binding antibody, for reducing systemic exposure of a directly-labeled immunoSPECT antibody to provide pharmacologic insight on both imaging and biotherapeutic dosing strategies. Assessment of tumor-to-blood ratios is relevant to diagnostic imaging agents and certain biotherapeutic applications, but additional considerations are required for intracellular drug delivery of toxic payloads. For instance, target-independent uptake and catabolism of conventional IgG-based antibody–drug conjugates by nonspecific pinocytosis likely contributes to normal tissue toxicity (31). Exploiting the accelerated systemic clearance of fragments that undergo renal filtration may reduce pinocytosis in most tissues by reducing plasma exposure, but at the cost of high renal uptake and low efficiency of payload delivery to tumor. Moreover, FcRn mutation of full-length IgG is not an ideal platform for optimizing toxin delivery either because the mechanism for increased clearance relies on blocking the recycling ability of FcRn after internalization to achieve widespread elimination

via endothelial cells throughout the body, most evident by the increased uptake and catabolism in liver and spleen. Nevertheless, the use of rapidly clearing antibody-based vehicles for drug delivery of potent payloads may be relevant to therapeutic index by limiting the degree of nonspecific pinocytosis in normal tissues, assuming that clearance organ uptake—whether kidney, liver, or otherwise—is tolerated.

Although both methods were successful in reducing exposure, engineering of HAHQ mutations into our antibody was more efficient than adding anti-gD-YTE-KF in terms of the reduction in systemic blood pool (**Fig. 3**), even when considering the deliberate 24-hour time delay. We could have coadministered the anti-gD-YTE-KF simultaneously with our labeled anti-HER2 antibodies to compare the FcRn binding attenuation and the competitive FcRn binding blockade methods at matched time points. However, we opted to investigate a staggered dosing interval to allow more time for efficient tumor uptake before modulating exposure, and reduce the amount of hepatic/splenic accumulation expected on the basis of our previous results with HAHQ mutant antibodies (20).

Our secondary goal was to reduce the undesirable click reaction of ^{111}In-labeled tetrazine that we previously encountered in pretargeted imaging with circulating TCO-modified antibodies (15), while still considering potential therapeutic implications (14). We considered that FcRn binding attenuation might induce undesirable accumulation in liver and spleen, the prominent tissue sites of IgG degradation in the absence of FcRn protection (20). However, based on prior dual isotope biodistribution studies (20), we hypothesized that rapid intracellular degradation in these sites would limit the amount of extracellular mAb-TCO_6 below the levels necessary for appreciable click reaction.

Our results with parental 7C2-TCO_6 using this approach were consistent with our previous work (15), reinforcing that the slow internalization of HER2 (32) and constant cell surface receptor pool allow efficient tumor click reaction. However, pretargeted imaging with 7C2-HAHQ-TCO_6 resulted in greater hepatic and splenic uptake than anticipated (**Figs. 2**, **5**, group 5). Even though the systemic levels of 7C2-HAHQ-TCO_6 were more than twice lower than those of 7C2-TCO_6 at 24 hours (**Fig. 3**), it led to sufficient levels of systemic click reaction, some of which distributed to these tissues. Accordingly, only a modest reduction in systemic blood pool activity was observed at 15 minutes after ^{111}In-labeled tetrazine with the HAHQ group relative to parental (10.1 $\pm$ 0.9 and 13.6 $\pm$ 1.4%ID/mL, respectively; Supplementary Fig. S4).

Administering ^{111}In-labeled tetrazine 48 hours (rather than 24 hours) after mAb-TCO_6 (when levels of 7C2-HAHQ-TCO_6 are four-fold lower relative to 7C2-TCO_6) may have reduced systemic click reaction, but lower tumor cell surface mAb-TCO_6 may have negated the potential benefits. Furthermore, mice receiving the anti-gD-YTE-KF clearing agent did experience a 48-hour time delay between mAb-TCO_6 and tetrazine; results showed similar levels of ^{111}In in whole blood, lower in tumor (**Fig. 5**, group 6), and lower in liver and spleen, albeit giving good tumor imaging on the day after tetrazine (**Fig. 2**, group 6).

Our study adds to the relatively small literature on examining the tumor uptake of full IgG with attenuated FcRn binding affinity (18, 19, 22, 33, 34). Notably, Burvenich and colleagues reported moderate to high tumor uptake, depending on the engineered mutations, of ^{111}In-labeled antibodies, but with very limited SPECT imaging data (33). Olafsen and colleagues (34) demonstrated lower tumor uptake using minibodies (~80 kDa) and scFv-Fc variants (~105 kDa, with HAHQ mutation); their renal uptake was inversely proportional to tumor uptake (~28 and 13%ID/g for minibody and scFv-Fc, respectively). It is possible that our use of an even larger molecule (~150 kDa) promoted higher tumor uptake by reducing renal clearance.

Consistent with the findings of Swiercz and colleagues (22), we observed that administering an antibody containing the YTE-KF mutation increased contrast. These effects on pharmacokinetics may be explained by this mutation yielding an IgG variant with single-digit nanomolar binding affinity to mouse FcRn at both extracellular and lysosomal pH (21). An antibody fragment (efgartigimod) engineered with "ABDEG" technology to treat autoimmune disorders has demonstrated similar effects in cynomolgus monkeys and in healthy volunteers (35), suggesting that clinical feasibility for imaging applications is within grasp. Our IgG-based clearing agent with the same mutations accelerated antibody clearance from the point of administration (**Fig. 3**) and preserved tumor uptake in direct imaging (**Figs. 2**, **4B**, group 3). However, these benefits came at the expense of waiting an additional day until image acquisition, and despite producing a favorable next-day image (**Fig. 2**, group 6), the clearing agent was less useful in the pretargeting study arm as it worsened tumor uptake (**Fig. 5B**). We postulate that the additional 24 hours delay allowed depletion of cell surface HER2 receptors available for click reaction, which decreased tumor uptake. However, this delay also improved contrast relative to images without clearing agent by increasing the time between mAb-TCO_6 and tetrazine, further demonstrating the importance of timing in pretargeted imaging.

Conclusion

Herein, we have applied pharmacokinetic modulation via FcRn binding mutations or a competitive clearing agent to both direct and pretargeted SPECT imaging with a full-length antibody to gain insight into pharmacologic implications for the corresponding biotherapeutic and/or potent immunoconjugates thereof. Tumor delineation against background in an internalizing, high HER2 expressing model could be achieved using directly labeled antibodies irrespective of FcRn recycling. However, results from imaging with directly labeled antibodies benefited more from reducing exposure via Fc point mutation or using an FcRn competitive clearing agent than with pretargeted imaging. Overall, both the HAHQ mutations and YTE-KF clearing agent approaches provided improved tumor-to-blood ratios, but each improvement came at a cost: HAHQ mutations with higher spleen and liver uptake, and YTE-KF clearing agent with the additional delay in image acquisition.

Disclosure of Potential Conflicts of Interest

L. Nazarova is an employees/paid consulting of Postdoctoral Research Fellow at Genentech. D. Mandikian is a Scientist at Genentech, Inc. G.Z. Ferl is a Sr. Scientist at Genentech, Inc.; has ownership interest (including patents) in Roche Stock. J.T. Koerber is a senior scientist at Genentech, Inc.; reports of receiving other commercial research support at Genentech, Inc. J. Ernst is a senior scientist at Genentech, Inc.; is a senior director at Xencor; has ownership interest (including patents) in Genentech, Inc. and Xencor. C.A. Boswell is a senior scientist at Genentech, Inc. No potential conflicts of interest were disclosed by the other authors.

Authors' Contributions

Conception and design: L. Nazarova, H. Rafidi, J.T. Koerber, J.D. Sadowsky, C.A. Boswell

Development of methodology: H. Rafidi, D. Mandikian, J. Ernst, J.D. Sadowsky, C.A. Boswell

Acquisition of data (provided animals, acquired and managed patients, provided facilities, etc.): L. Nazarova, H. Rafidi, J.T. Koerber, S. Ulufatu, J. Ho, J. Lau, S.-F. Yu
Analysis and interpretation of data (e.g., statistical analysis, biostatistics, computational analysis): L. Nazarova, H. Rafidi, D. Mandikian, G.Z. Ferl, J.T. Koerber, C.A. Boswell
Writing, review, and/or revision of the manuscript: L. Nazarova, H. Rafidi, D. Mandikian, G.Z. Ferl, C.W. Davies, S.-F. Yu, J.D. Sadowsky, C.A. Boswell
Administrative, technical, or material support (i.e., reporting or organizing data, constructing databases): J. Ernst, J.D. Sadowsky, C.A. Boswell
Study supervision: H. Rafidi, S. Ulufatu
Other (designed and contributed antibody reagents): C.W. Davies

Acknowledgments

This work was internally funded by Genentech/Roche. We acknowledge Ruedi Port and Simon Williams for helpful discussions.

The costs of publication of this article were defrayed in part by the payment of page charges. This article must therefore be hereby marked *advertisement* in accordance with 18 U.S.C. Section 1734 solely to indicate this fact.

Received October 24, 2019; revised January 7, 2020; accepted January 28, 2020; published first February 5, 2020.

References

1. Ryman JT, Meibohm B. Pharmacokinetics of monoclonal antibodies. CPT Pharmacometrics Syst Pharmacol 2017;6:576–88.
2. Wang W, Wang EQ, Balthasar JP. Monoclonal antibody pharmacokinetics and pharmacodynamics. Clin Pharmacol Ther 2008;84:548–58.
3. Lamberts LE, Williams SP, Terwisscha van Scheltinga AG, Lub-de Hooge MN, Schroder CP, Gietema JA, et al. Antibody positron emission tomography imaging in anticancer drug development. J Clin Oncol 2015;33:1491–504.
4. Boswell CA, Brechbiel MW. Development of radioimmunotherapeutic and diagnostic antibodies: an inside-out view. Nucl Med Biol 2007;34:757–78.
5. Covell DG, Barbet J, Holton OD, Black CD, Parker RJ, Weinstein JN. Pharmacokinetics of monoclonal immunoglobulin G1, F(ab')2, and Fab' in mice. Cancer Res 1986;46:3969–78.
6. Holton OD 3rd, Black CD, Parker RJ, Covell DG, Barbet J, Sieber SM, et al. Biodistribution of monoclonal IgG1, F(ab')2, and Fab' in mice after intravenous injection. Comparison between anti-B cell (anti-Lyb8.2) and irrelevant (MOPC-21) antibodies. J Immunol 1987;139:3041–9.
7. Tsai SW, Li L, Williams LE, Anderson AL, Raubitschek AA, Shively JE. Metabolism and renal clearance of ^{111}In-labeled DOTA-conjugated antibody fragments. Bioconjug Chem 2001;12:264–70.
8. Pandit-Taskar N, O'Donoghue JA, Ruan S, Lyashchenko SK, Carrasquillo JA, Heller G, et al. First-in-human imaging with ^{89}Zr-Df-IAB2M Anti-PSMA minibody in patients with metastatic prostate cancer: pharmacokinetics, biodistribution, dosimetry, and lesion uptake. J Nucl Med 2016;57:1858–64.
9. Olafsen T, Sirk SJ, Olma S, Shen CK, Wu AM. ImmunoPET using engineered antibody fragments: fluorine-18 labeled diabodies for same-day imaging. Tumour Biol 2012;33:669–77.
10. Vegt E, de Jong M, Wetzels JF, Masereeuw R, Melis M, Oyen WJ, et al. Renal toxicity of radiolabeled peptides and antibody fragments: mechanisms, impact on radionuclide therapy, and strategies for prevention. J Nucl Med 2010;51:1049–58.
11. Arano Y, Fujioka Y, Akizawa H, Ono M, Uehara T, Wakisaka K, et al. Chemical design of radiolabeled antibody fragments for low renal radioactivity levels. Cancer Res 1999;59:128–34.
12. Altai M, Membreno R, Cook B, Tolmachev V, Zeglis B. Pretargeted imaging and therapy. J Nucl Med 2017;58:1553–9.
13. Oliveira BL, Guo Z, Bernardes GJL. Inverse electron demand Diels-Alder reactions in chemical biology. Chem Soc Rev 2017;46:4895–950.
14. Rossin R, van Duijnhoven SM, Ten Hoeve W, Janssen HM, Kleijn LH, Hoeben FJ, et al. Triggered drug release from an antibody-drug conjugate using fast "Click-to-Release" chemistry in mice. Bioconjug Chem 2016;27:1697–706.
15. Mandikian D, Rafidi H, Adhikari P, Venkatraman P, Nazarova L, Fung G, et al. Site-specific conjugation allows modulation of click reaction stoichiometry for pretargeted SPECT imaging. mAbs 2018;10:1269–80.
16. Rossin R, Lappchen T, van den Bosch SM, Laforest R, Robillard MS. Diels-Alder reaction for tumor pretargeting: in vivo chemistry can boost tumor radiation dose compared with directly labeled antibody. J Nucl Med 2013;54:1989–95.
17. Olafsen T, Kenanova VE, Wu AM. Tunable pharmacokinetics: modifying the in vivo half-life of antibodies by directed mutagenesis of the Fc fragment. Nat Protoc 2006;1:2048–60.
18. Kenanova V, Olafsen T, Crow DM, Sundaresan G, Subbarayan M, Carter NH, et al. Tailoring the pharmacokinetics and positron emission tomography imaging properties of anti-carcinoembryonic antigen single-chain Fv-Fc antibody fragments. Cancer Res 2005;65:622–31.
19. Kenanova V, Olafsen T, Williams LE, Ruel NH, Longmate J, Yazaki PJ, et al. Radioiodinated versus radiometal-labeled anti-carcinoembryonic antigen single-chain Fv-Fc antibody fragments: optimal pharmacokinetics for therapy. Cancer Res 2007;67:718–26.
20. Yip V, Palma E, Tesar DB, Mundo EE, Bumbaca D, Torres EK, et al. Quantitative cumulative biodistribution of antibodies in mice: effect of modulating binding affinity to the neonatal Fc receptor. mAbs 2014;6:689–96.
21. Vaccaro C, Zhou J, Ober RJ, Ward ES. Engineering the Fc region of immunoglobulin G to modulate in vivo antibody levels. Nat Biotechnol 2005;23:1283–8.
22. Swiercz R, Chiguru S, Tahmasbi A, Ramezani SM, Hao G, Challa DK, et al. Use of Fc-engineered antibodies as clearing agents to increase contrast during PET. J Nucl Med 2014;55:1204–7.
23. Chen X, Dennis M, Junutula JR, Phillips GL, Pillow TH, Sliwkowski XM, et al. , inventors; Genentech Inc., assignee. Anti-HER2 antibodies and immunoconjugates. US Patent 9,518,118B2, 2016 Dec 13.
24. Ohri R, Bhakta S, Fourie-O'Donohue A, Dela Cruz-Chuh J, Tsai SP, Cook R, et al. High-throughput cysteine scanning to identify stable antibody conjugation sites for maleimide- and disulfide-based linkers. Bioconjug Chem 2018;29:473–85.
25. Junutula JR, Raab H, Clark S, Bhakta S, Leipold DD, Weir S, et al. Site-specific conjugation of a cytotoxic drug to an antibody improves the therapeutic index. Nat Biotechnol 2008;26:925–32.
26. Rondon A, Ty N, Bequignat JB, Quintana M, Briat A, Witkowski T, et al. Antibody PEGylation in bioorthogonal pretargeting with trans-cyclooctene/tetrazine cycloaddition: in vitro and in vivo evaluation in colorectal cancer models. Sci Rep 2017;7:14918.
27. Chizzonite R, Truitt T, Podlaski FJ, Wolitzky AG, Quinn PM, Nunes P, et al. IL-12: monoclonal antibodies specific for the 40-kDa subunit block receptor binding and biologic activity on activated human lymphoblasts. J Immunol 1991;147:1548–56.
28. Zeglis BM, Mohindra P, Weissmann GI, Divilov V, Hilderbrand SA, Weissleder R, et al. Modular strategy for the construction of radiometalated antibodies for positron emission tomography based on inverse electron demand Diels-Alder click chemistry. Bioconjug Chem 2011;22:2048–59.
29. Barrett PH, Bell BM, Cobelli C, Golde H, Schumitzky A, Vicini P, et al. SAAM II: simulation, analysis, and modeling software for tracer and pharmacokinetic studies. Metabolism 1998;47:484–92.
30. Boswell CA, Marik J, Elowson MJ, Reyes NA, Ulufatu S, Bumbaca D, et al. Enhanced tumor retention of a radiohalogen label for site-specific modification of antibodies. J Med Chem 2013;56:9418–26.
31. Polakis P. Antibody drug conjugates for cancer therapy. Pharmacol Rev 2016;68:3–19.
32. Austin CD, De Maziere AM, Pisacane PI, van Dijk SM, Eigenbrot C, Sliwkowski MX, et al. Endocytosis and sorting of ErbB2 and the site of action of cancer therapeutics trastuzumab and geldanamycin. Mol Biol Cell 2004;15:5268–82.
33. Burvenich IJ, Lee FT, O'Keefe GJ, Makris D, Cao D, Gong S, et al. Engineering anti-Lewis-Y hu3S193 antibodies with improved therapeutic ratio for radioimmunotherapy of epithelial cancers. EJNMMI Res 2016;6:26.
34. Olafsen T, Kenanova VE, Sundaresan G, Anderson AL, Crow D, Yazaki PJ, et al. Optimizing radiolabeled engineered anti-p185HER2 antibody fragments for in vivo imaging. Cancer Res 2005;65:5907–16.
35. Ulrichts P, Guglietta A, Dreier T, van Bragt T, Hanssens V, Hofman E, et al. Neonatal Fc receptor antagonist efgartigimod safely and sustainably reduces IgGs in humans. J Clin Invest 2018;128:4372–86.